Metallurgical Transactions 20A (1989) 1037-1054

11. COMPARISON OF THE ABRASIVE WEAR PROPERTIES OF STELLITE HARDFACING ALLOYS DEPOSITED BY ARC WELDING AND LASER CLADDING

Re S. Atamert and H K D H Bhadeshia

11.1 Introduction

In Chapter 10 the presence of systematic microstructural and microanalytical differences were demonstrated between Stellite cobalt-based hardfacing alloys deposited by manual metal arc welding, tungsten inert gas (TIG) welding and laser cladding, using typical process parameters. As a consequence of the differences in nominal heat input (920, 660 and 240 Jmm^{-1} for MMA, TIG and laser cladding, respectively) and associated freezing rates, the scale of the microstructure and the degree of dilution was found to decrease in the order MMA, TIG and laser cladding, with the hardness increasing in the same order. Microanalysis experiments also suggested that the TIG deposits are most uniform with respect to chemical compositions, and due to their relatively high matrix iron content, tend to be most stable to the transformation from the face-centered cubic (fcc) to hexagonal close-packed (hcp) phase. Hence, the TIG samples were to contain lower densities of intrinsic stacking faults when compared with the MMA and laser clad samples.

This chapter is an attempt to relate the differences summarised above, and the detailed differences reported in Chapter 10, between the three kinds of hardfacing deposits, to the wear properties. The aim is to attempt a rationalisation of wear behaviour as a function of microstructure and abrasive characteristics. Detailed microscopy is used to deduce the micromechanisms of wear.

11.2 Experimental Method

Most of the experimental details have been presented in Chapter 10, so that the following section deals with just the additional techniques associated with the wear analysis.

Abrasion wear tests (pin-on-disc) were performed on 3mm diameter cylindrical specimens impinging vertically on a rotating disc coated with the appropriate abrasive. The specimens were gravity loaded with a mass of 450g. The cylindrical samples were spark-machined from the weld deposits, so that the test surface was parallel to the layers of hardfacing material. The test surfaces had to be flattened by grinding in order to remove the curvature associated with the top surfaces of the weld deposits. This entailed removal of ≈ 0.5mm of the top surface so that all tests begin at this depth below the surface.

The weight loss due to abrasive wear was measured at various intervals during the test period. The effects of two kinds of fixed-abrasives were studied using the rotating coated disc test: 280 mesh SiC, and 400 mesh Al_2O_3 with nominal particle sizes ≈ 40 and ≈ 17 μm respectively (see Fig. 7.1). The relative velocity of the disc and sample was 0.63 m/s. This sliding speed would probably cause a local rise in temperature ahead of abrasive particles. However, in similar

circumstances, the bulk temperature has been reported to rise by only $10^{o}C$.[1] In any case, the effect would be applicable to all samples and consequently does not influence the comparisons between samples. In order to avoid spurious effects due to the degradation of abrasive during the wear tests, the abrasive paper was changed at 1 minute intervals. The wear tests were carried out in air under dry test conditions.

In addition to the pin-on-disc tests, single and multiple scratch tests were carried out using SiC fibres ($\approx$ 100μm diameter) loaded with a mass of 100g, and with a Vicker's pyramidal diamond loaded at 100, 500 and 1000g. The scratch tool was in each case mounted at the end of a balanced parallelogram arm instrumented with strain gauges and loaded by gravity. The specimen was then moved linearly by a geared electric motor at a speed of $0.25mms^{-1}$ for a distance of 7mm.

The worn surfaces were ultrasonically cleaned and then examined using a scanning electron microscope. Thin foil samples for transmission electron microscopy were prepared as in Chapter 10, but the aim here was to examine the fine structure in the vicinity of abraded surfaces. The samples were extracted by slicing parallel to the abraded surfaces, lightly levelling the abraded surface with 1200 mesh SiC polishing paper, and then grinding back from the opposite surface to reach a thickness suitable for electropolishing. The levelling may have caused some additional deformation. However, the use of the much finer SiC, the wet conditions and the light pressure should ensure that any additional deformation effect is small. It is estimated that the samples examined represent a depth of about 0.6mm below the abraded surface concerned.

11.3 Results and Discussion

11.3.1 Pin-on-Disc Abrasion Tests

11.3.1.1 Alumina Abrasive

It is well established that variations in wear resistance are related to the difference in hardness of the abrasive and resisting surfaces. If the difference is small, the rate of material removal during abrasion is found to be very low when compared with the case where the abrasive is relatively hard.[2] The critical value of the ratio of the abrasive hardness to that of the strained hardened metal surface (H_a/H_m) has been estimated empirically as 1.2, below which an effective increase in wear resistance is observed.[3]

In the present study, Al_2O_3 and SiC abrasives were chosen in order to compare the effect of the hardness and the size of the abrasives and to examine material removal mechanisms under each abrasive. The hardness of Al_2O_3, SiC and $(Fe, Cr)_7C_3$ is 2100, 2480-2600 and 1200-1600 HV respectively.[4,5]

Weight loss versus time curves of the abrasion test results with the Al_2O_3 abrasive for the MMA, TIG and laser clad samples are given in Fig. 11.1a with corresponding worn surface micrographs being presented in Figs. 11.1b-e. The mean wear rates of the MMA, TIG and laser

clad samples are found to be 0.0068, 0.0029 and 0.0032 g/min. The results show that the MMA weld has the poorest abrasive wear resistance among the three deposits, with a wear rate which remains constant throughout the test, unlike the other two samples which at least initially exhibited a decreasing wear rate with time.

Although the TIG sample initially showed a lower net weight loss when compared with the laser clad sample, its wear rate was found to increase significantly after 4 minutes of abrasion. In fact, the ultimate weight losses for the TIG and laser clad samples were observed to be similar. The observed rise in wear rate towards that end of the test, for both the TIG and laser clad samples corresponds approximately to the point where it is the diluted regions of the deposit which are being abraded, since the undiluted layers have then been completely eroded. Hence, the design life of the cladding should strictly be calculated on the basis of the undiluted layer thickness.

Scanning electron microscopy (Fig. 11.1b-e) revealed that the worn surfaces of the MMA and the laser clad deposits were neatly cut by the abrasive particles, in a manner consistent with micromachining processes. The wear grooves can in these cases be seen to be continuous and smooth, indicating that the material which was originally within the grooves was neatly cut away and detached by the abrasive particles. Consistent with their higher wear rate, the grooves tended to be deeper for the MMA samples reflecting their lower starting strength. Indeed, the observed constant wear rate (i.e., the linear relationship between the weight loss and time plot) of the MMA samples is indicative of an inadequate degree of strain hardening during the abrasion test. The rate of strain hardening is known to increase as the microstructure becomes refined,[8] so that the lack of sufficient strain hardening is attributed to the relative coarseness of the MMA deposit microstructure, as reported in Chapter 10.

The fact that the laser and TIG samples showed better wear resistance than the MMA sample again correlates with their higher starting hardness, and to the finer scale of their microstructures (Chapter 10). As will be discussed later, these microstructural features are also of importance in controlling the spread of deformation in the vicinity of the grooves. It is notable that only the laser sample showed an increase in wear resistance during the progress of the test: the MMA sample is relatively soft and has a coarse microstructure, whereas the TIG sample has a relatively high matrix stacking fault energy (corresponding to its higher matrix iron content) which leads to a lower work hardening rate.[8]

The TIG sample, which showed the best initial resistance to wear, also exhibited a drastically different worn surface morphology (Fig. 11.1d,e). The relatively discontinuous grooves are in this case not formed by pure cutting, the material exhibiting clear resistance to the passage of the abrasive particles. Material debris can be seen to be piled up at intervals, apparently at positions within the grooves where the motion of the abrasive particles has been stifled. The alloy clearly behaves in a more ductile manner so that the micromachining debris does not readily detach from the test surface and hinder the wear process. The higher ductility relative to the laser sample

cannot be attributed to the minor difference in the scale of the two microstructures. It is more likely that the laser sample, due to its lower matrix stacking fault energy, strain hardens rapidly so that its harder debris easily detaches during wear, giving rise to "free machining" behaviour. Due to its higher matrix iron concentration, the TIG samples have a higher stacking fault energy and consequently strain harden to a lesser degree, giving a more ductile machining behaviour.

11.3.1.2 Silicon Carbide Abrasive

Similar experiments were carried out using the harder (≈ 2480-2600HV)[4,5] SiC abrasive. Weight-loss versus time curves, and scanning electron microscope observations of the final worn surfaces are given in Fig. 11.2. The results are clearly different from the case where the abrasive particles were alumina: the samples this time show more similar wear rates, the mean values of which are 0.0100, 0.0094 and 0.0086 g/min for the MMA, TIG and laser clad specimens respectively. Apart from minor fluctuations, they all exhibit an approximately constant wear rate during the test, although the laser samples start off with slightly lower wear rate, perhaps a reflection of their strain hardening capacity. Consistent with these observations, the wear surfaces (Fig. 12.2b-d) all show neat, continuous grooves with the samples offering little resistance to the passage of abrasive particles. Clearly, the use of a SiC abrasive has wiped out most of the differences between the three kinds of samples. The wear rates obtained with the SiC abrasive is higher than that with Al_2O_3 abrasive. This can be attributed to two effects, the most important of which is the size effect.[7-13] The abrasives used in this study are in a size range where the wear rate increases with abrasive size; the SiC abrasive is coarse compared with the alumina. The higher hardness of SiC may also contribute to its more aggressive abrasion properties, but this is likely to be a smaller effect since both SiC and Al_2O_3 have a significantly higher hardness when compared with the phases present in the Stellite deposits. It is estimated that in the case of the laser and TIG samples, the top, undiluted layers are removed completely after about 2-3 minutes of testing.

11.3.2 Transmission Electron Microscopy

Thin foils for transmission electron microscopy were prepared directly from the abraded surfaces, after the pin-on-disc tests carried out using SiC abrasives. The metallographic results presented here are representative of three samples examined from each of the abraded deposits. Nonetheless, it is recognised that the observations reported here are essentially qualitative and are intended to reflect the broad trends in deformation behaviour.

The results are illustrated in Figs. 11.3-11.5. The matrix (originally of face-centered cubic structure) regions of the MMA and laser clad deposits were found to contain numerous platelets of hexagonal close-packed structure, due to stress induced fcc→hcp transformation. The frequency of occurrence of the platelets was highest for the laser clad samples. This contrasted with the TIG samples, which seemed to contain much more dislocation debris, with very few hcp platelets, although twinned fcc regions could often be observed. The behaviour of the TIG sample is as

expected, since its matrix phase has a high stacking fault energy corresponding to its relatively high iron content.

The fact that the MMA deposits contain a lower density of hcp platelets relative to the laser samples is at first sight confusing since the matrix chemical compositions of the two samples are very similar. However, the MMA deposit has a lower starting hardness, and it will be demonstrated later that the deformation associated with the abrasion process extends over a larger volume for the MMA deposit (due to the coarseness of its microstructure). Both of these factors would lead to lower mean levels of stress in the material, so that a lower degree of stress induced transformation is expected. The fact that the laser clad samples are unique in exhibiting an increase in wear resistance during testing (Fig. 11.1) can now be explained, since the platelets formed by fcc→hcp transformation offer formidable obstacles to dislocation motion, leading to considerable strain hardening.

11.3.3 Scratch Tests Using Vickers Diamond

Scratch tests were carried out using a Vickers pyramidal diamond indenter with 100, 500 and 1000g loads, for all three kinds of samples, although no significant differences in abrasive behaviour were found for the different loads used. After scratching, the specimens were examined using scanning electron microscopy (Fig. 11.6). The results clearly illustrate the considerable deformation (in the form of slip bands) induced in the region adjacent to the scratches. The extent of the deformation increases with applied load (Figs. 11.6a,b). At the highest load used, 1000g, clear signs of matrix cracking were observed (Fig. 11.6c). For a given load, the degree of deformation in the vicinity of the scratch was noted to be largest for the MMA samples, consistent with their coarse microstructure (Figs. 11.6b,d,e). The slip bands were seen to be impeded by the presence of eutectic carbides, although this did not completely prevent the onset of deformation in the Co-rich matrix which was separated from the scratches by the network of eutectic carbide (Fig. 11.6). The spread of deformation occurred to a lesser degree for both the TIG and laser clad samples; while the slip bands could be seen all along the length of the scratches in the MMA samples, they tended to be discontinuous for the TIG and laser clad samples, reflecting the finer scale of the microstructure.

The critical role of the matrix in supporting the carbide phase was emphasised by deep-etching the samples to allow the carbides to protrude from the surface; these samples were then scratched, (100g, Vickers pyramidal diamond, Fig. 11.7a), and subjected to impact (Fig. 11.7b). The carbide particles were observed to fracture and collapse into heaps of particles (Fig. 11.7). Subsurface deformation is clear as seen from Fig. 11.8 when the scratch test was carried out using SiC fiber.

11.4 Conclusions

The abrasive wear properties of manual metal arc welded, tungsten inert gas welded and laser clad Stellite 6 hardfacing deposits have been studied and related to microstructural differences. With alumina abrasives, the wear resistance was found to increase in the order MMA→laser clad→TIG samples. The MMA samples are worst because of their coarser microstructure and lower starting hardness. The TIG samples have the highest initial wear resistance because of their higher ductility and matrix stacking fault energy. During wear, the laser clad samples were found to be the only ones to exhibit an initial increase in wear resistance, due to the relatively low stacking fault energy of the matrix phase.

The effect of using a coarser and harder silicon carbide abrasive was to increase the wear rate in all samples; the increase is largest for the the laser and TIG samples. In fact the samples all showed very similar wear rates when tested with the silicon carbide abrasive.

This observed wear behaviour could be correlated directly with the structure of the worn surface and of the underlying regions.

Finally, it must be emphasised that the present study was deliberately conducted on samples prepared using what are believed to be *typical* process parameters. There are numerous such parameters which can be adjusted in order to alter the properties of a deposit for any single process. Indeed, it may even be the case that the chemical composition which is suited to a given process may not be good for another process. We therefore make no attempt to rank the processes in any order of excellence; such a ranking would in any case be futile since the choice of process must be highly application dependent.

11.5 References

1) A. P. MERCER: ' The effects of atmospheric humidity and oxygen on the wear of metals by fine abrasives ', Ph.D. Thesis, October 1985, University of Cambridge.
2) E. RABINOWICZ: in Proc. Conf. 'Wear of Materials 1983', 1983, ASME, New York, 12.
3) R. C. D. RICHARDSON: Wear, 1968, **11**, 245.
4) "Handbook of Physics and Chemistry", ed. R. C. Weast, 57 edition, CRC Press, Ohio, 1976.
5) T. S. EYRE: 'Wear Characteristics of Metals', Source Book on Wear Control Technology, ASM, 1978, pp.1-10.
6) R. W. K. HONEYCOMBE: "The Plastic Deformation of Metals", 2nd ed., 1984, Edward Arnold, London, pp.231-245.
7) M. A. MOORE: 'Abrasive Wear', in Proc. Conf. 'Fundamentals of Friction and Wear of Materials', 4-5 October 1980, Pittsburgh Pennsylvania, ASM.
8) S. W. DATE, and S. MALKIN: Wear, 1976, **40**, 223.
9) K. HOKKIRIGAWA, and K. KATO: Tribology International, 1988, **21**, 51.
10) L. E. SAMUELS: "Metallographic Polishing by Mechanical Methods", 2nd ed., 1971, Melbourne & London, pp.65-86.
11) J. LARSEN-BASSE: in Proc. Conf. 'Wear of Materials 1981', 1981, ASME, New York, 534.
12) J. LARSEN-BASSE: Wear, 1968, **12**, 35.
13) A. MISRA, and I. FINNIE: Wear, 1981, **65**, 359.

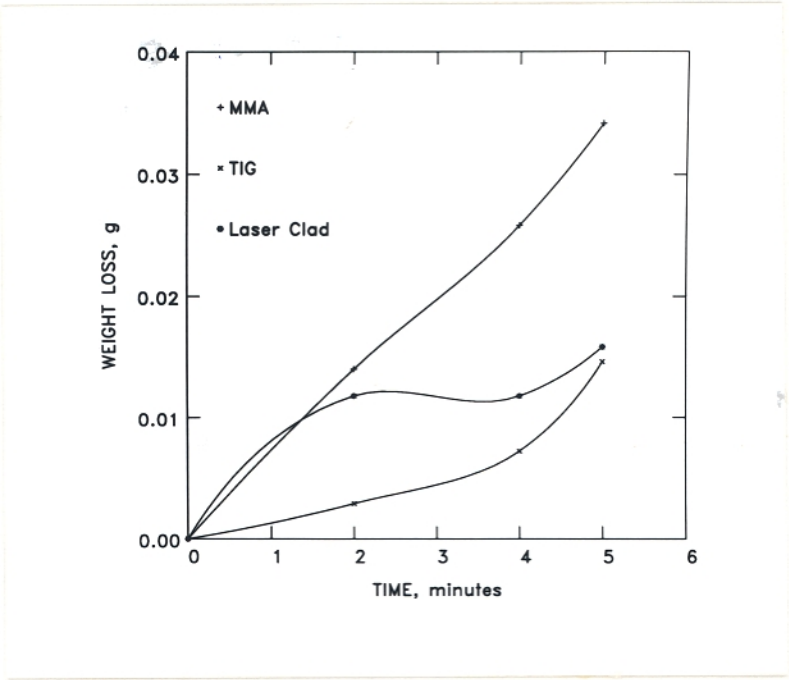

a

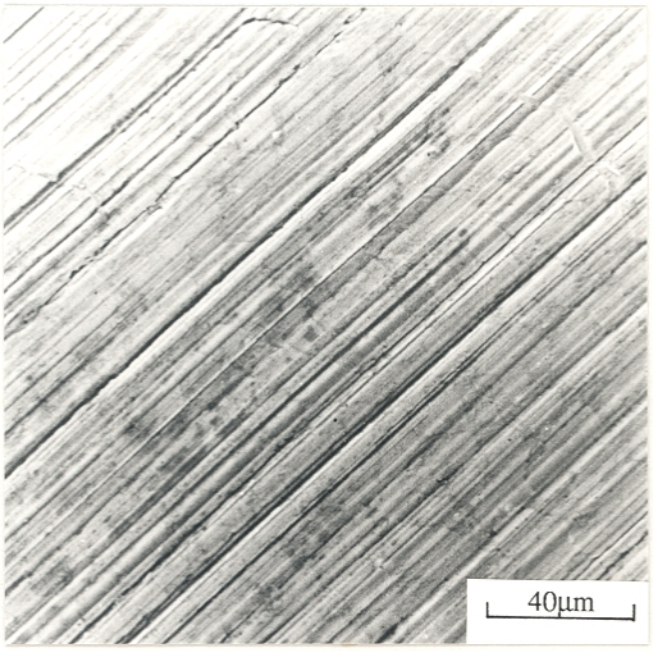

b

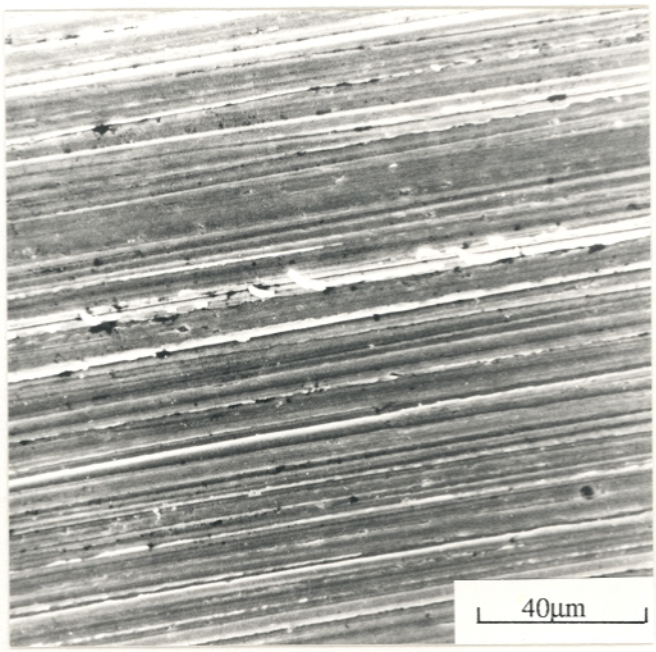

c

Fig. 11.1: a) Weight loss versus time curves, for wear tests done using alumina abrasive. Scanning electron micrographs of the final worn surfaces of b) MMA; c) laser clad sample and (d,e) TIG sample.

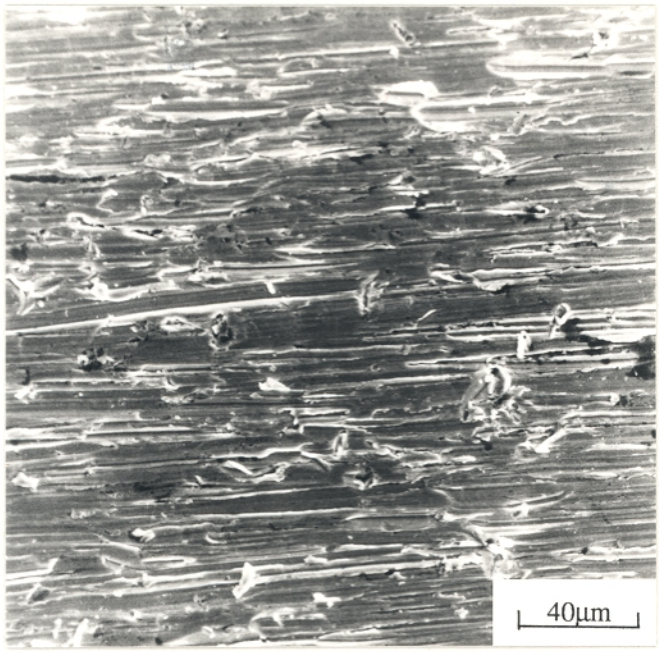

a

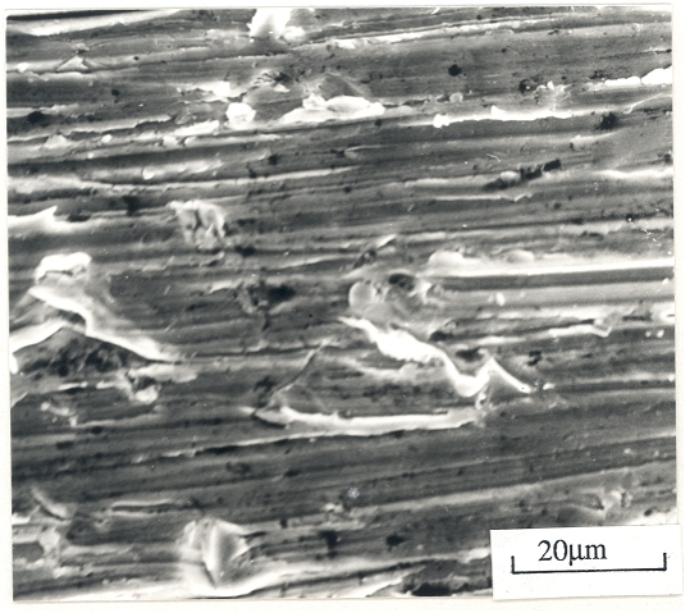

b

Fig. 11.1: a) Weight loss versus time curves, for wear tests done using alumina abrasive. Scanning electron micrographs of the final worn surfaces of b) MMA; c) laser clad sample and (d,e) TIG sample.

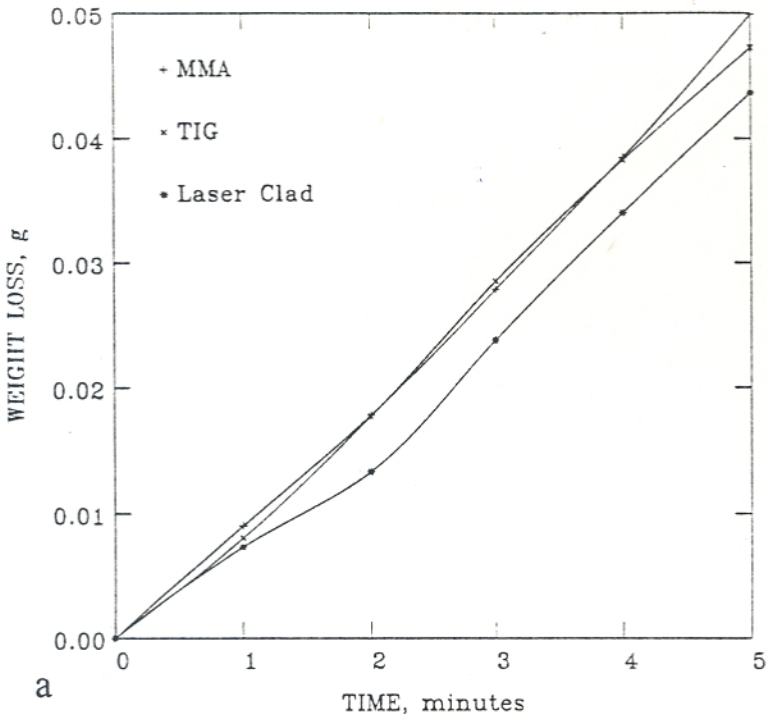

a

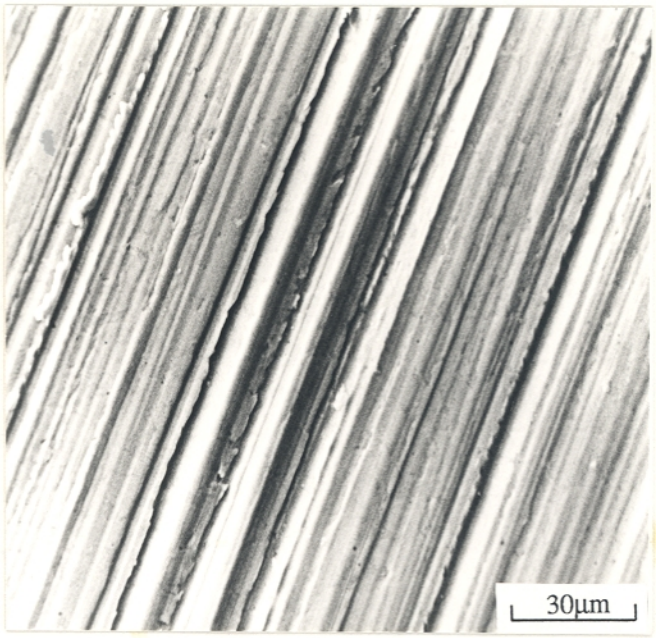

b

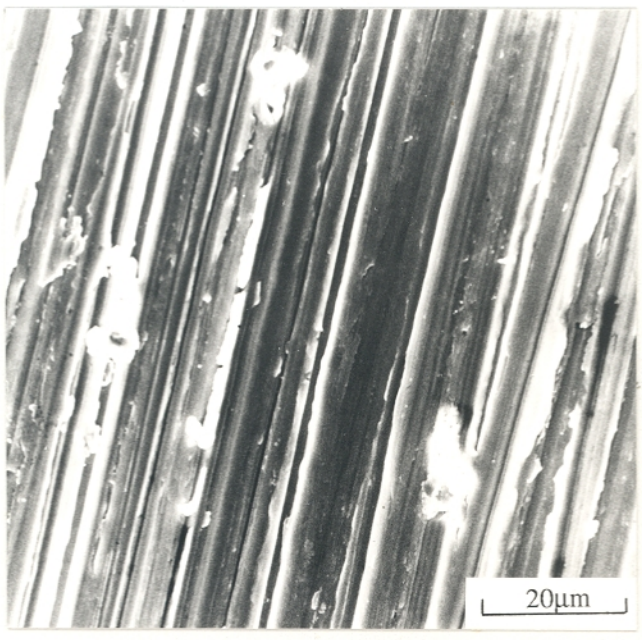

c

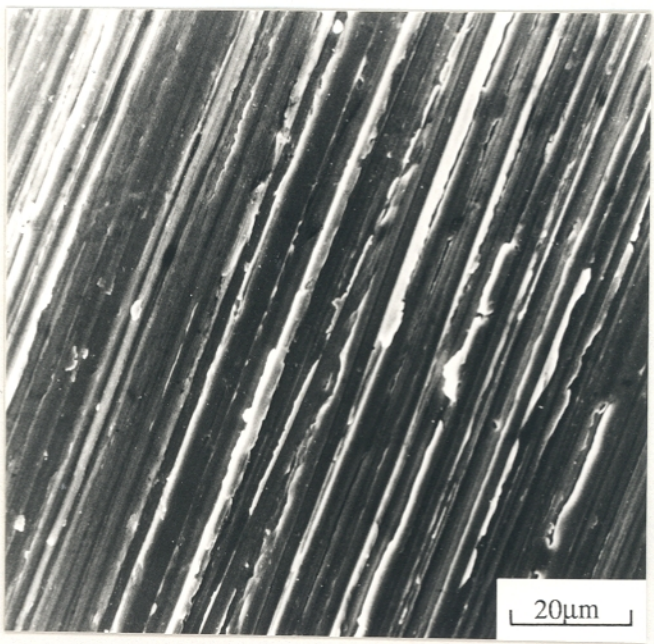

d

Fig. 11.2: a) Weight loss versus time curves, for wear tests done using silicon carbide abrasive; (b-d) scanning electron micrographs of the final worn surfaces of MMA, TIG and laser clad samples.

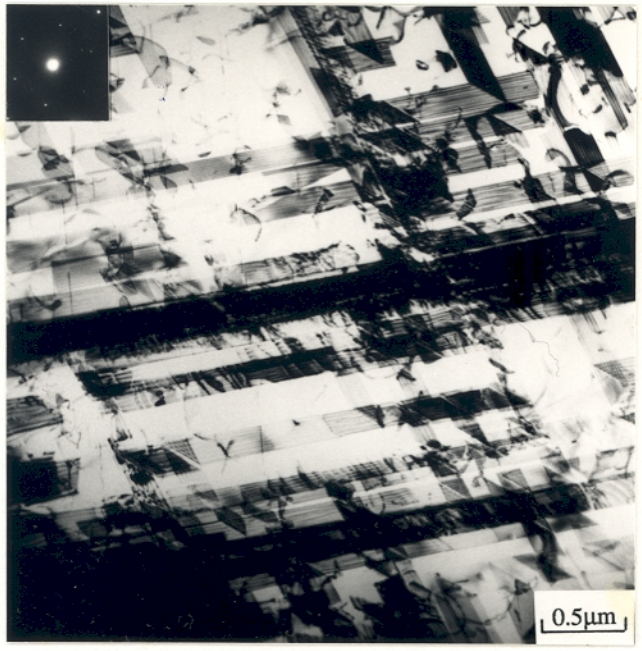

a

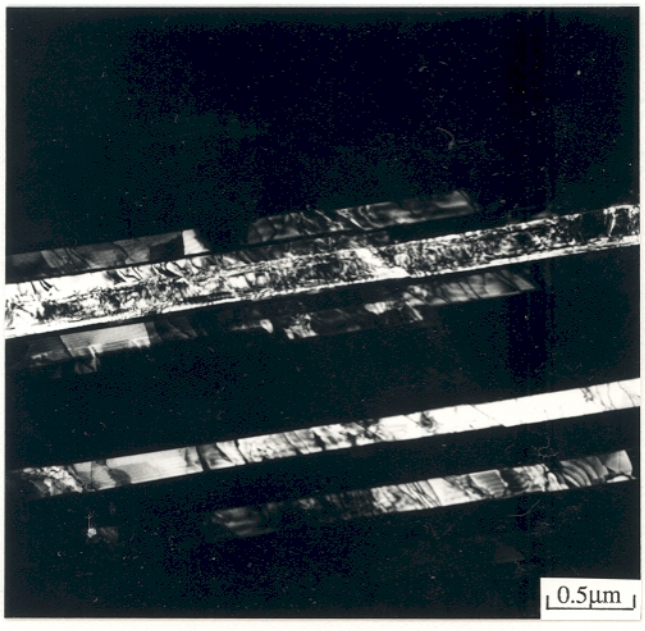

b

Fig. 11.3: Transmission electron micrographs from an abraded MMA sample: a) bright field image and electron diffraction pattern confirming the presence of hcp platelets ([0 0 0 1] zone axis); b) dark field image of hcp platelets.

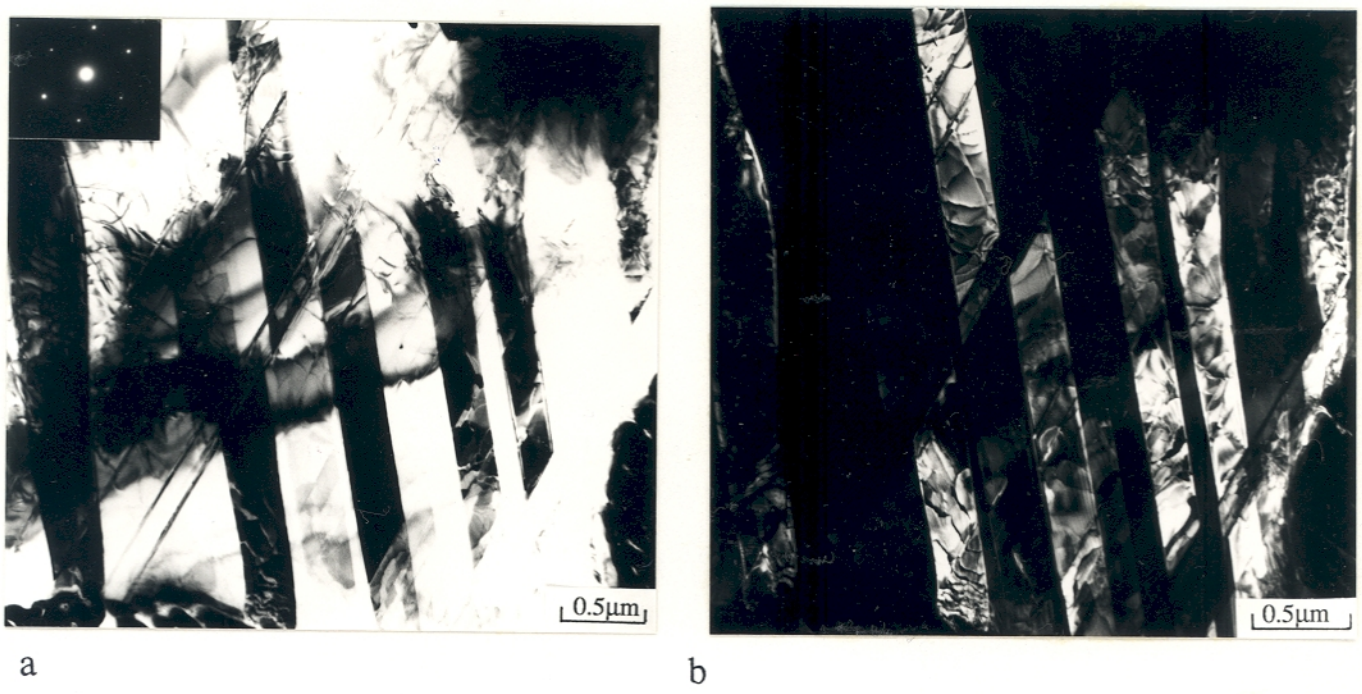

Fig. 11.4: Transmission electron micrographs from an abraded Laser clad sample: a) bright field image and electron diffraction pattern confirming the presence of hcp platelets ([1 $\bar{2}$ 1 $\bar{3}$] zone axis); b) dark field image of hcp platelets.

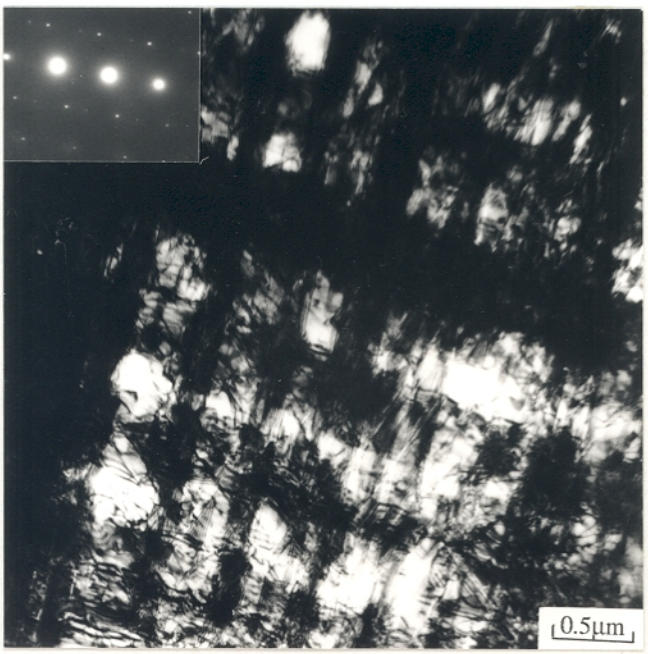

Fig. 11.5: Transmission electron micrograph from an abraded TIG specimen.

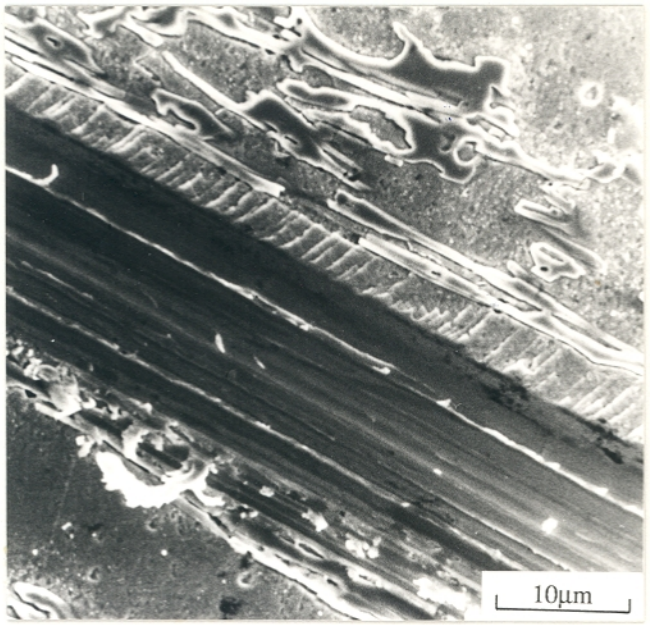

a

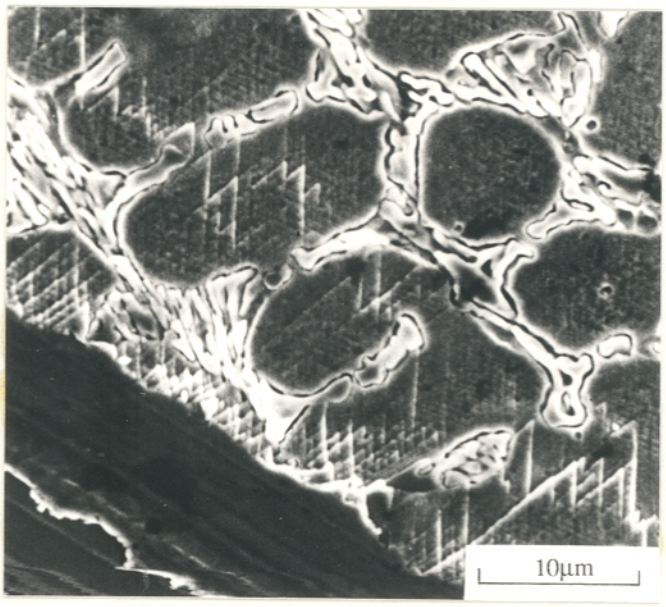

b

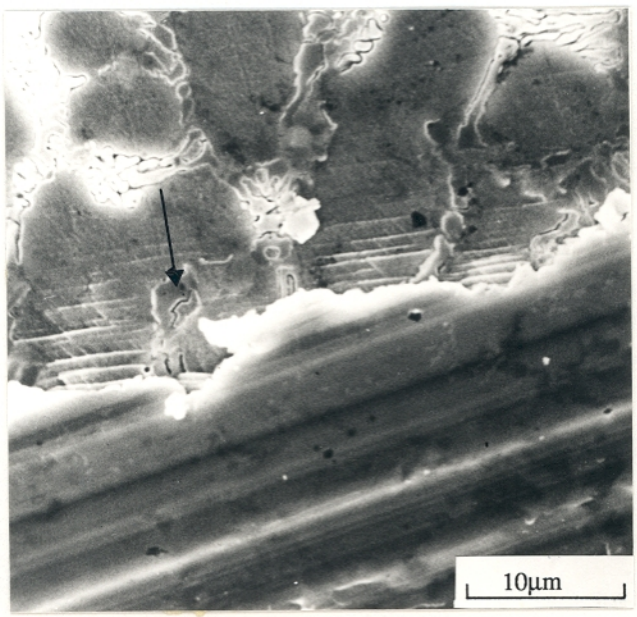

c

Fig. 11.6: Scanning electron micrographs from scratched specimens: a) MMA 100g; b) MMA 500g; c) MMA 1000g (arrow indicates the matrix cracking); d) TIG 500g; e) laser clad 500g.

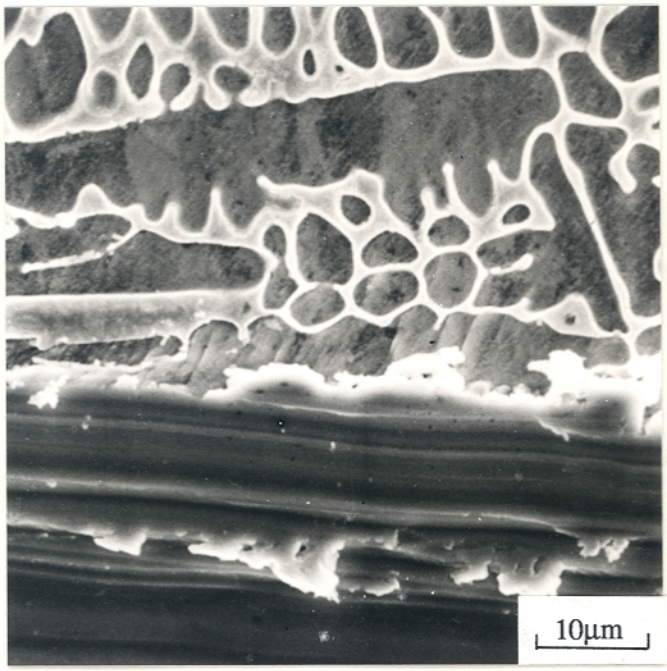

d

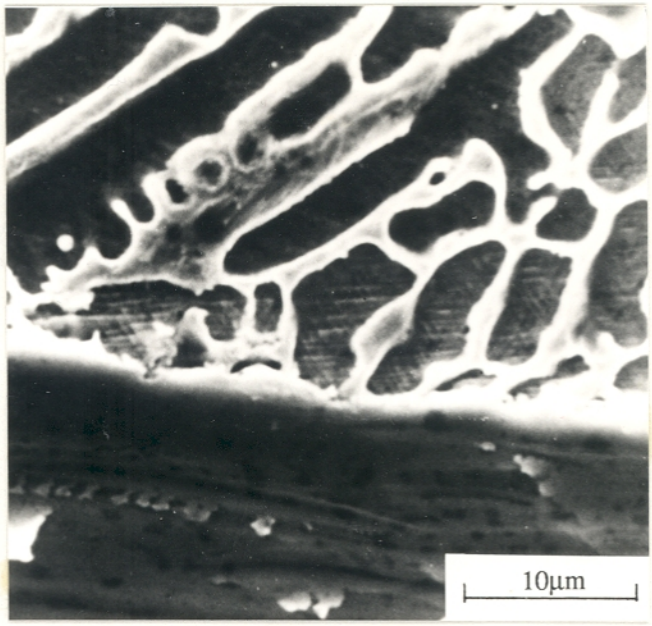

e

Fig. 11.6: Scanning electron micrographs from scratched specimens: a) MMA 100g; b) MMA 500g; c) MMA 1000g (arrow indicates the matrix cracking); d) TIG 500g; e) laser clad 500g.

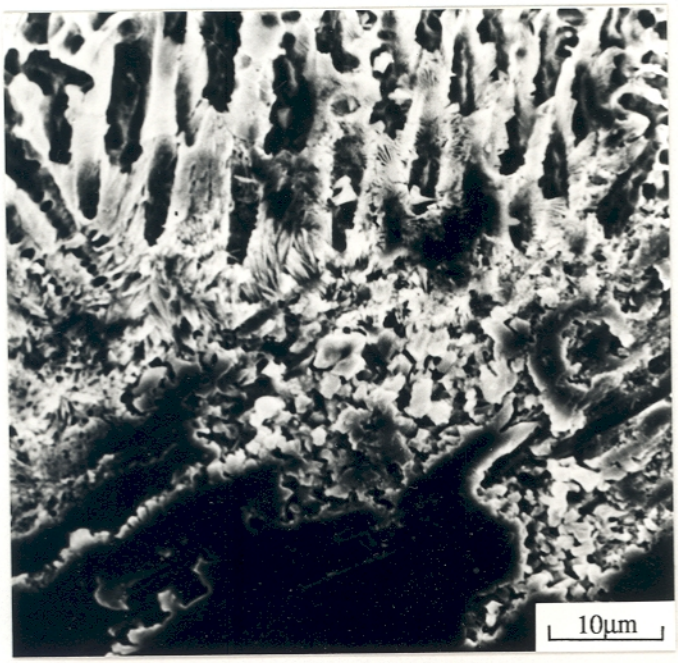

a

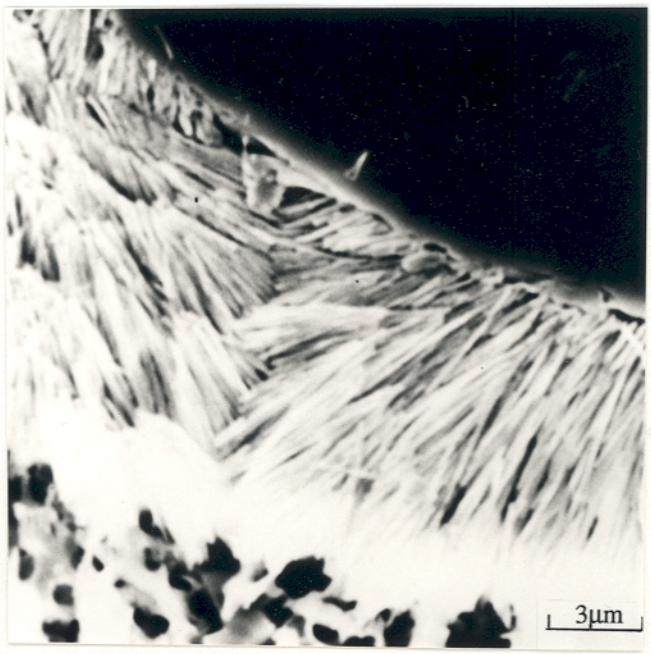

b

Fig. 11.7: Scanning electron micrographs from a deep-etched specimen which was subsequently a) scratched with a Vickers diamond; b) subjected to impact, illustrating the collapse of the unsupported eutectic carbides.

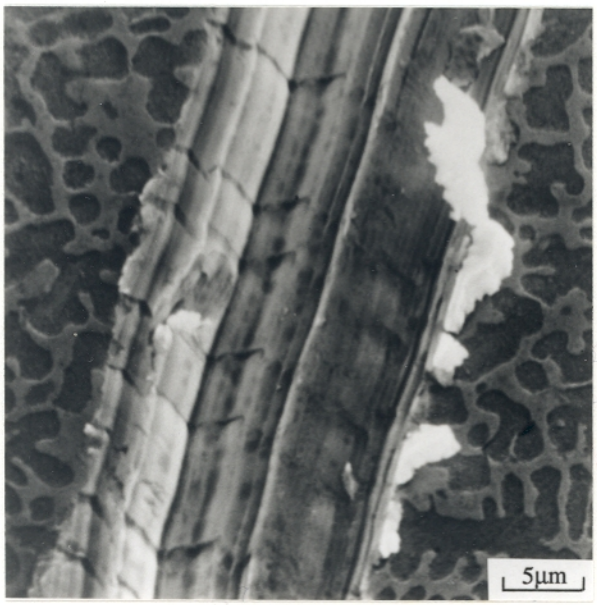

Fig. 11.8: Scanning electron micrograph from scratched specimen with 100g using SiC fiber (100µm), illustrating the subsurface deformation.